Substrate-assisted Enzymatic Formation of Lysinoalanine in Duramycin

Supplementary Information

List of supplementary figures and tables:

Supplementary Table 1. Crystallographic data collection and refinement statistics.

	DurN (6C0G)	DurN-3-Dha6Ala (6C0H)	DurN-duramycin (6C0Y)
Data collection			
Space group	$P4_12_12$	$P4_12_12$	P1
Cell dimensions			
a, *b*, *c* (Å)	57.6, 57.6, 146.9	40.0, 40.0, 303.4	59.9, 67.4, 69.1
α, β, γ (°)	90.0, 90.0, 90.0	90.0, 90.0, 90.0	71.5, 76.2, 72.9
Resolution (Å)*	53.63-2.15 (2.18-2.15)	39.65-1.90 (1.93-1.90)	64.72-1.66 (1.69-1.66)
R_{merge}*	0.101 (1.736)	0.078 (1.022)	0.072 (0.726)
$I / \sigma I$*	21.9 (2.3)	25.5 (2.2)	12.0 (2.1)
Completeness (%)*	100.0 (99.9)	100.0 (100.0)	95.8 (95.5)
Redundancy*	23.0 (24.2)	21.4 (14.6)	4.4 (4.4)
Refinement			
Resolution (Å)	53.63-2.15	75.84-1.90	64.72-1.66
No. reflections	14215	19755	104658
R_{work} / R_{free}	21.7/26.1	19.0/25.1	18.4/24.2
No. atoms			
Protein	1747	1739	6864
Ligand/ion	2	97	1085
Water	55	134	1223
B-factors			
Protein	52.1	35.6	21.1
Ligand/ion	38.9	33.4	22.2
Water	49.6	51.7	40.6
R.m.s. deviations			
Bond lengths (Å)	0.009	0.019	0.020
Bond angles (°)	1.160	1.851	2.119

*Diffraction data from a single crystal was used. *Values in parentheses are for highest-resolution shell.

Supplementary Table 2. Expected and observed masses of all compounds prepared for this study. All masses listed are exact mass values unless specified otherwise. The "S" prefix in the Figure Reference column refers to Supporting Information figures.

Number	Name (MALDI data unless otherwise indicated)	Expected Exact m/z (Da)	Observed Exact m/z (Da)	Error (ppm)	Figure Reference
4	[Compound **4** + 3H]$^{3+}$ ESI	768.0013	768.0041	-3.65	1c
5	[Compound **5** + 3H]$^{3+}$ ESI	819.3387	819.3420	-4.03	1c
6	[**3**-Dha6Ala + H]$^{+}$	2304.00	2303.84	69.44	S3a (SI)
7	[**Dur-FL** + H]$^{+}$	2370.89	2371.20	-130.75	S3b (SI)
8	[**3**-Hya15Ser + H]$^{+}$	2258.00	2258.01	-4.43	S3c (SI)
9	[**3**-Hya15Asp + H]$^{+}$	2287.00	2285.46	673.37	S3f (SI)
11	[Deoxyduramycin + H]$^{+}$	1997.85	1996.96	-55.06	S3g (SI)
12	[DurA coexpressed with DurM and DurN + H]$^{+}$	10418.49 (avg. mass)	10419.57 (avg. mass)	-103.66	S3d (SI)
12	[DurA coexpressed with DurM and DurN after DTT treatment + H]$^{+}$	10418.49 (avg. mass)	10419.15 (avg. mass)	-63.35	S3e (SI)

Supplementary Table 3. Primer sequences used in this work.

Primer Name	Primer Sequences (5'-3')
LA_pET28MBP-durorf7-ins_F	GTACTTCCAATCCGGCATGAAAAGCGCCAAGGAAC
LA_pET28MBP-durorf7-ins_R	CGGCCGCAAGCTTCAGGACGTCAGCCGG
LA_pMAL-2cx-DurLA-R17A_F	CATCGCCCGCATCCA
LA_pMAL-2cx-DurLA-R17A_R	TGCGGGCGATGATATCC
LA_DurN-R17K_F	CGTGGATATCATCAAACGCATCCAGGAGCTCATG
LA_DurN-R17K_R	GCTCCTGGATGCGTTTGATGATATCCACGTCCTG
LA_DurN_R18A_F	TATCATCCGCGCCATCCAGGAGCTCATGG
LA_DurN_R18A_R	GCTCCTGGATGGCGCGGATGATATCCACG
LA_DurN_R18E_F	GATATCATCCGCGAAATCCAGGAGCTCATGG
LA_DurN_R18E_R	GCTCCTGGATTTCGCGGATGATATCCACGTC
LA_pET-DurN-Q20A_V3_F	CATCCGCCGCATCGCCGAGCTCATGGTTCTGTGCTC
LA_pET-DurN-Q20A_V3_R	CCATGAGCTCGGCGATGCGGCGGATGATATCCACG
LA_DurN-W68A_V3-F	CGCGACGAAGGCCGCCCTCGAGACCCTG
LA_DurN-W68A_V3-R	CAGGGTCTCGAGGGCGGCCTTCGTCGCG
LA_DurN_Q89A_F	GGTCGCCTGGGCAAACAAGAGCGAGAACATG
LA_DurN_Q89A_R	CGCTCTTGTTTGCCCAGGCGACCAGTTCCTTC
LA_pMAL-2cx-DurLA-E101A_F	TTCGTGCCCTCAAGAACG
LA_pMAL-2cx-DurLA-E101A_R	CTTGAGGGCACGAATGG
LA_DurN_E106A_F	CAAGAACGCCGCACAGCAATCCGGCATCAC
LA_DurN_E106A_R	CGGATTGCTGTGCGGCGTTCTTGAGTTCAC
LA_DurA(K2R)_1_R_v2	CTGCAGCTCTGGCGGCAGGCGAAG
LA_DurA(K2R)_2_F)_v2	CTTCGCCTGCCGCCAGAGCTGCAG
LA_DurA(S6A)_1_R	GAACGGGCCGAAGGCGCAGCTCTGC
LA_DurA(S6A)_2_F	GCAGAGCTGCGCCTTCGGCCCGTTC
LA_DurA(D15S)_1_R	CCTGTTACTTGGTGTTGCCGCTACACACGAAGG
LA_DurA(D15S)_2_F	GTTCACCTTCGTGTGTAGCGGCAACACCAAG
DurN_F_LICv1	TACTTCCAATCCAATGCAATGAAAAGCGCCAAGGAACCGACGATCTACCA
DurN_R_LICv1	TTATCCACTTCCAATGTTATTATCAGGACGTCAGCCGGGCGACC

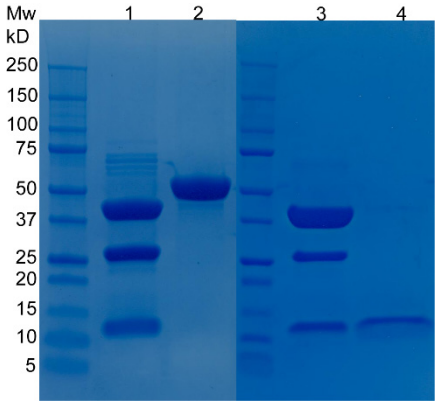

Supplementary Figure 1 | DurN purification and tag removal. DurN was purified as an N-terminal MBP fusion protein (lane 2, 56 kDa); The His-tagged MBP was removed by TEV digestion (lanes 1 & 3, tag-free DurN is 13.5 kDa, TEV protease is 27 kDa, and MBP is 42.5 kDa); further purification of TEV-digested MBP-DurN by removal of MBP with a nickel affinity column gives tag-free DurN (lane 4). Purification was performed independently three times with similar results.

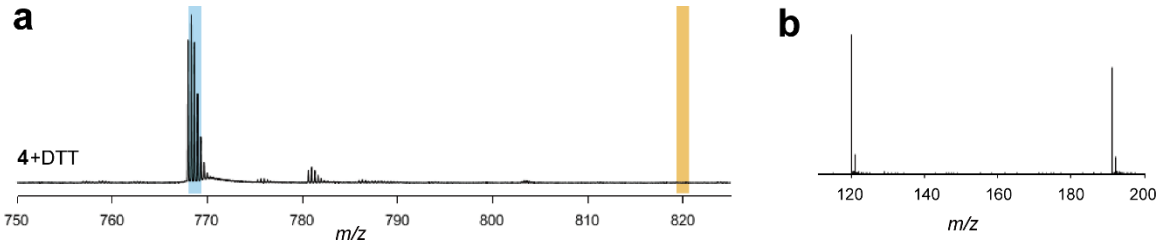

Supplementary Figure 2 | LC-MS analysis of a positive control for compound 4. a, *in vivo* prepared compound **4 (**by coexpression of DurA, DurM, DurX, and DurN and then treated with Glu-C) was incubated with DTT, followed by LC-MS analysis. **b**, LC-MS/MS of compound **4**. The y1 fragment ion (see text) is no observed. Experiment was performed independently three times with similar results.

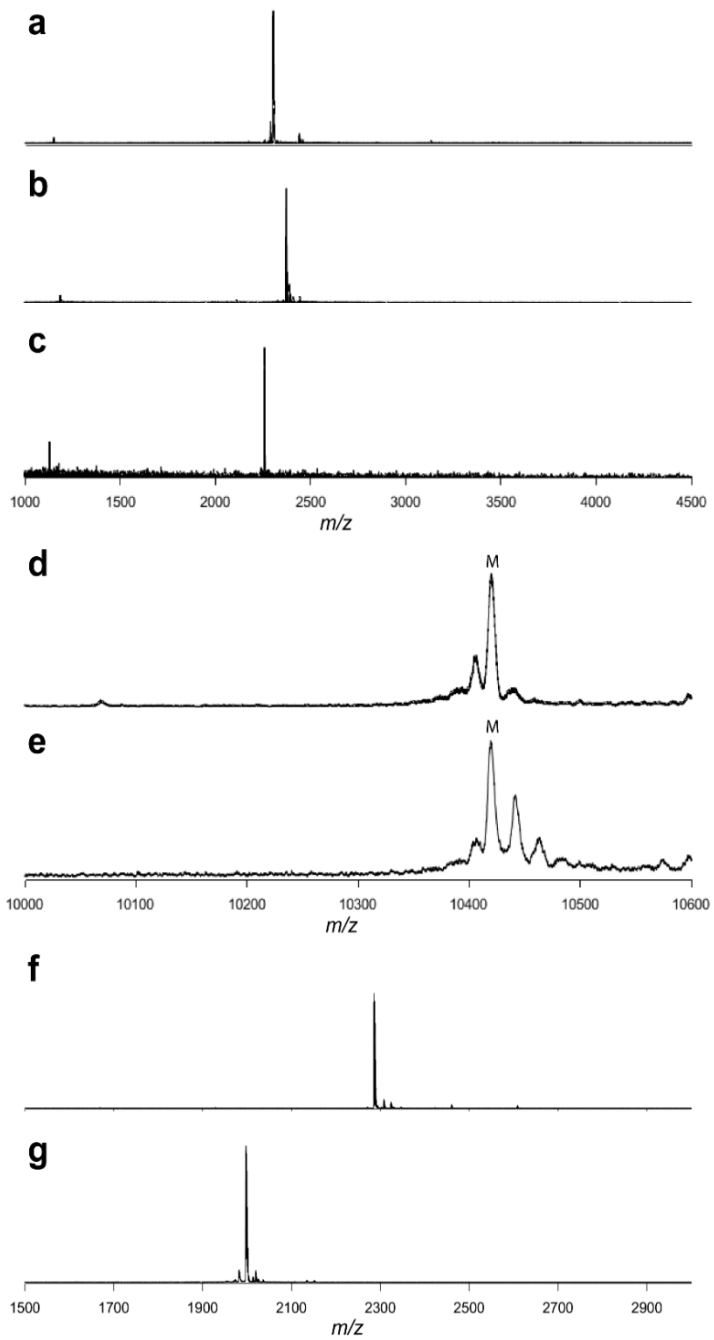

Supplementary Figure 3 | Preparation of duramycin analogs. a-g, MALDI-TOF mass spectra of compounds **3**-Dha6Ala (**a**), Dur-FL (**b**), **3**-Hya15Ser (**c**), and deoxyduramycin (**g**) produced in *E. coli.* (**d**) MALDI-TOF mass spectrum showing full-length DurA after coexpression with DurM and DurN; (**e**) The full-length product was treated with DTT and no DTT adduct was observed, indicating Lal was formed; (**f**) full-length peptide was digested by endoproteinase GluC to remove most of the LP. (**g**) the material in panel **f** was digested by aminopeptidase to remove the residual residues from the LP yielding deoxyduramycin. Expected and observed masses are listed in Supplementary Table 2. All preparations were performed three times independently. Representative data is shown.

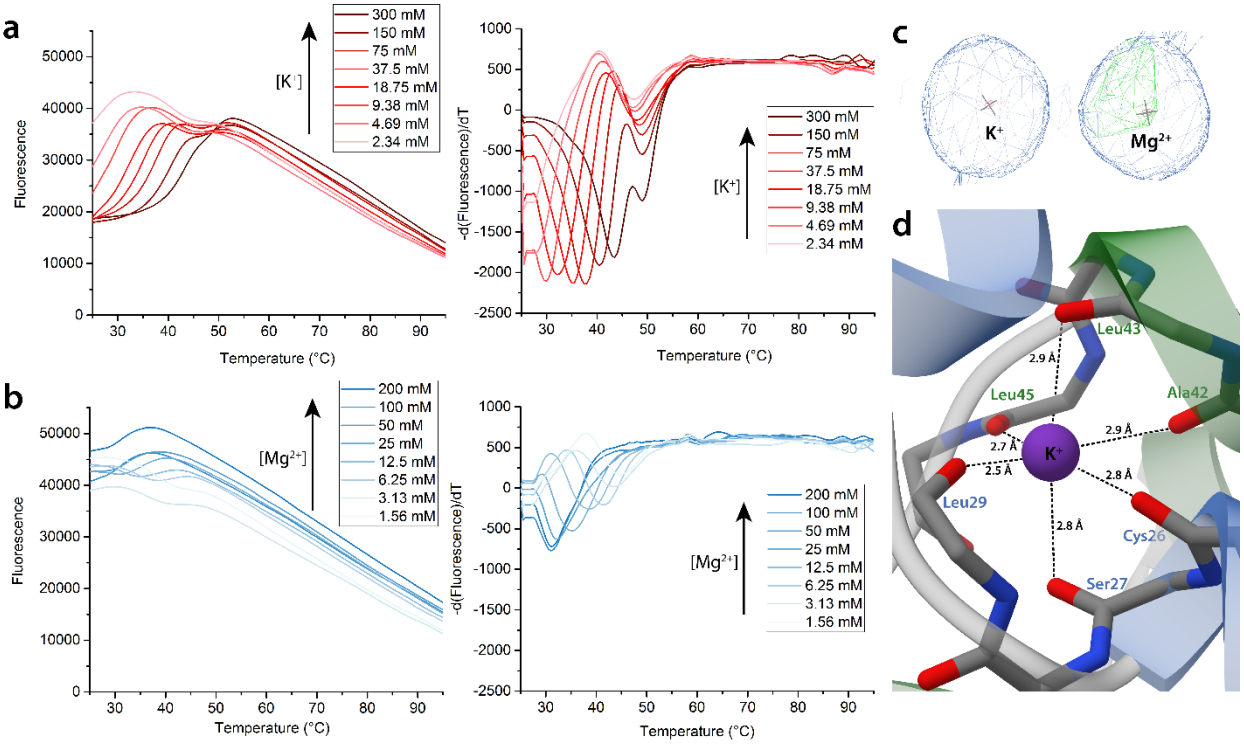

Supplementary Figure 4 | Melt curves, negative first derivatives of the melt curves obtained by differential scanning fluorimetry (DSF), and potassium coordination by DurN. a, DSF data corresponding to DurN in the presence of increasing potassium ion concentrations (2.34 mM – 300 mM). The dose-dependent stabilization of DurN by potassium ions is made evident by the increasing melting temperature as a function of potassium ion concentration (i.e. right-shifting inflection point in the left panel and minima in the right panel). **b,** Similar DSF data corresponding to DurN in the presence of increasing magnesium ion concentration (i.e. 1.56 mM – 200 mM). No appreciable difference in the melt curves and persistence of high initial fluorescence across all magnesium ion concentrations suggests that DurN thermal stability is not influenced by magnesium ion concentration. **c**, $2F_o - F_c$ maps (blue) at 1.5σ and positive $F_o - F_c$ maps (green) at 3σ of one structural ion binding site when potassium or magnesium ions are modeled and refined in REFMAC5 (Vagin, A.A. et al. REFMAC5 dictionary: organization of prior chemical knowledge and guidelines for its use. *Acta Crystallogr. D Biol. Crystallogr.* **60**, 2184-2195 (2004)). **d**, Octahedral potassium ion coordination by DurN involving amide carbonyl oxygen ligands from the DurN backbone of both monomers color-coded green or light blue. Experiments were performed once, but are supported by potassium requirement for activity and stability and MD simulations.

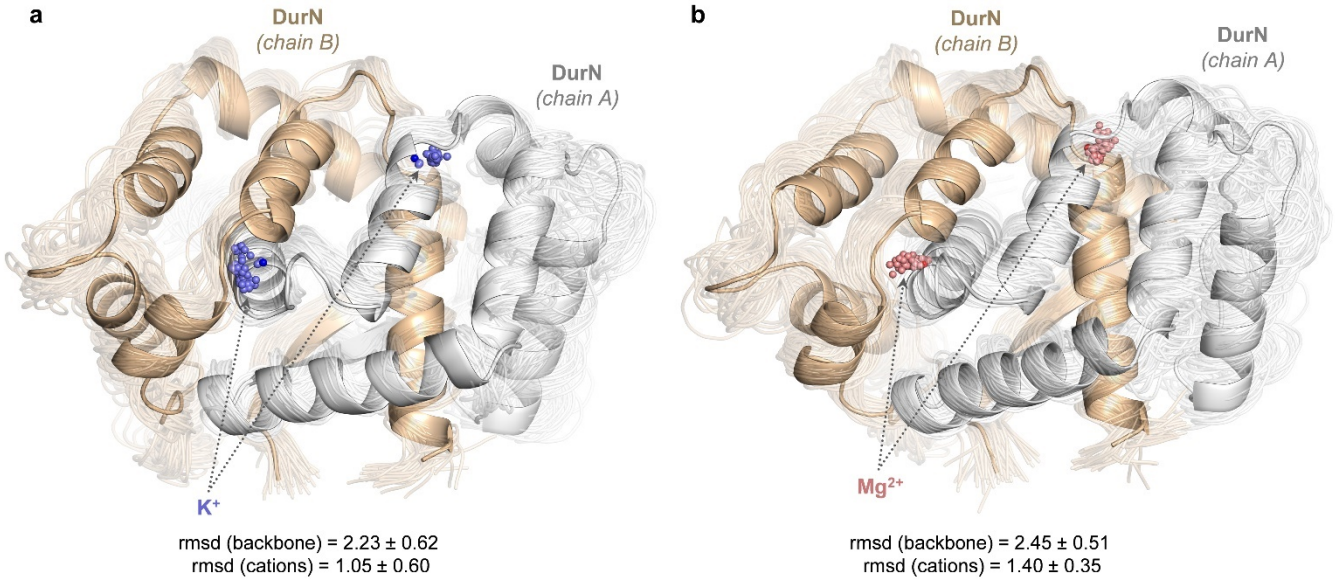

Supplementary Figure 5 | Effects of structural cations on the structure and dynamics of the DurN homodimer investigated through MD simulations. DurN was modeled in the *apo* state and two different cations, **a**, potassium (shown as blue spheres) and **b**, magnesium (shown as red spheres) were considered. Conformational ensembles for both models show 50 superimposed snapshots derived from 1.0 μs trajectories and are displayed as partially transparent cartoons. The crystallographic structure of DurN is shown as a solid cartoon as a reference. The crystallographic positions of the cations are represented as dark blue (for K^+) and dark red (for Mg^{2+}) spheres. Average root-mean-square deviations (rmsd) for the protein backbone and cations are shown in angstroms. Simulations show that potassium ions fluctuate less in the metal binding site and reduce the flexibility of the DurN homodimer compared to magnesium ions. This observation, together with the crystallographic and differential scanning fluorimetry (DSF) data, strongly suggest preferential binding of K^+ at the homodimer interface.

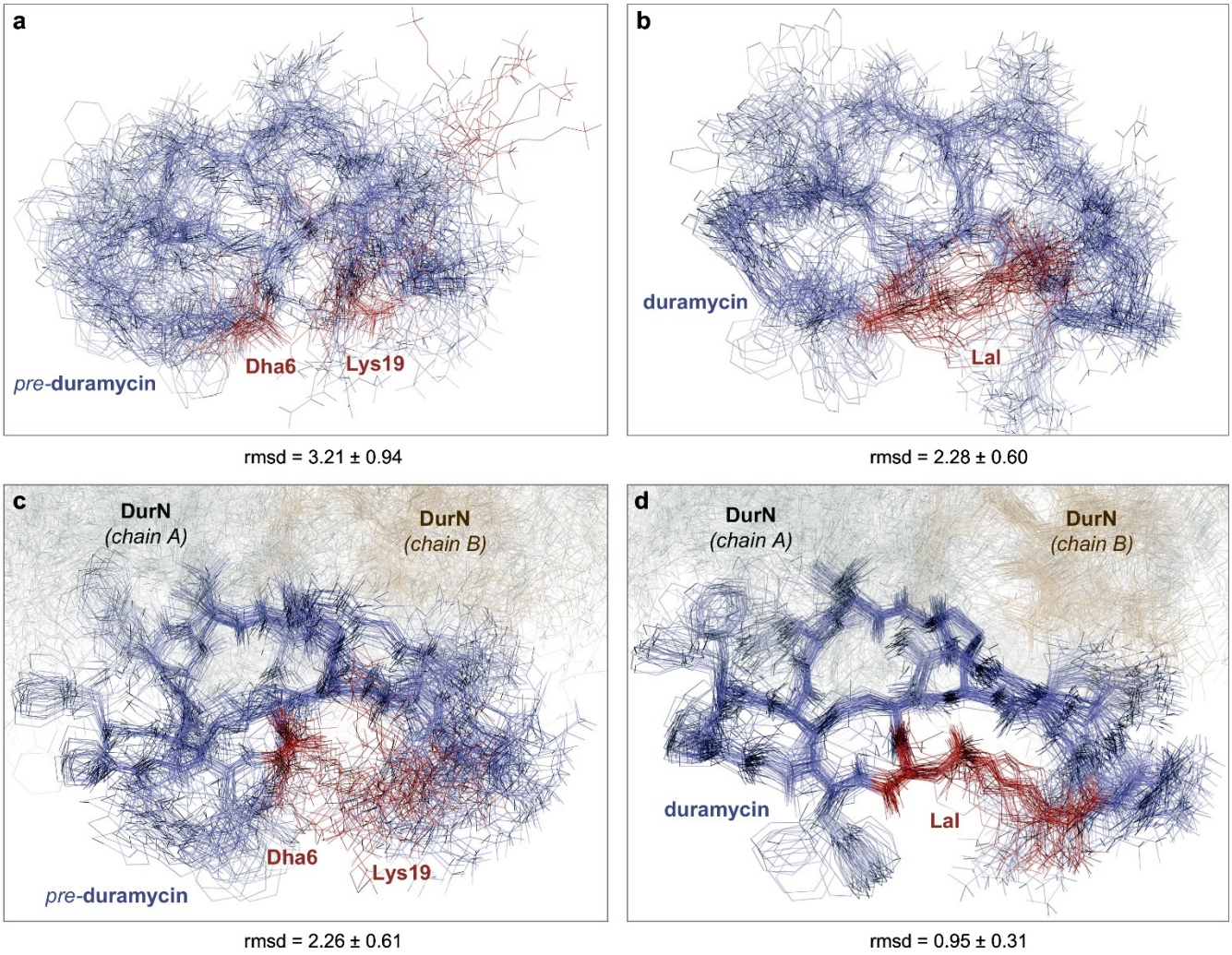

Supplementary Figure 6 | Structure and dynamics of duramycin in solution and bound to DurN examined through MD simulations. Conformational ensembles for all models show 50 superimposed snapshots derived from 1.0 μs trajectories. Substrate backbone and sidechains are shown as dark and light blue lines, respectively. Lysinoalanine (Lal) and unbridged Dha6 and Lys19 are shown as red lines. DurN is shown as grey (chain A) and brown (chain B) lines. Hydrogens have been omitted for clarity. Average root-mean-square deviations (rmsd) for the substrate backbone are shown in angstrom. Free uncyclized *pre*-duramycin (**a**) and (duramycin, **b**) are very flexible in solution. Binding to DurN significantly reduces the flexibility of both peptides (**c**,**d**), particularly duramycin which shows a quite rigidified backbone.

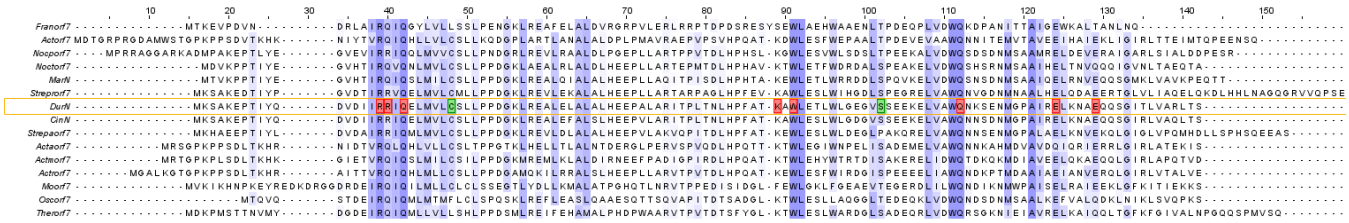

Supplementary Figure 7 | Multiple sequence alignment of DurN and its homologs. DurN is highlighted in the orange box. Residues that resulted in inactive variants when mutated to Ala are highlighted in red and those that remained active are highlighted in green.

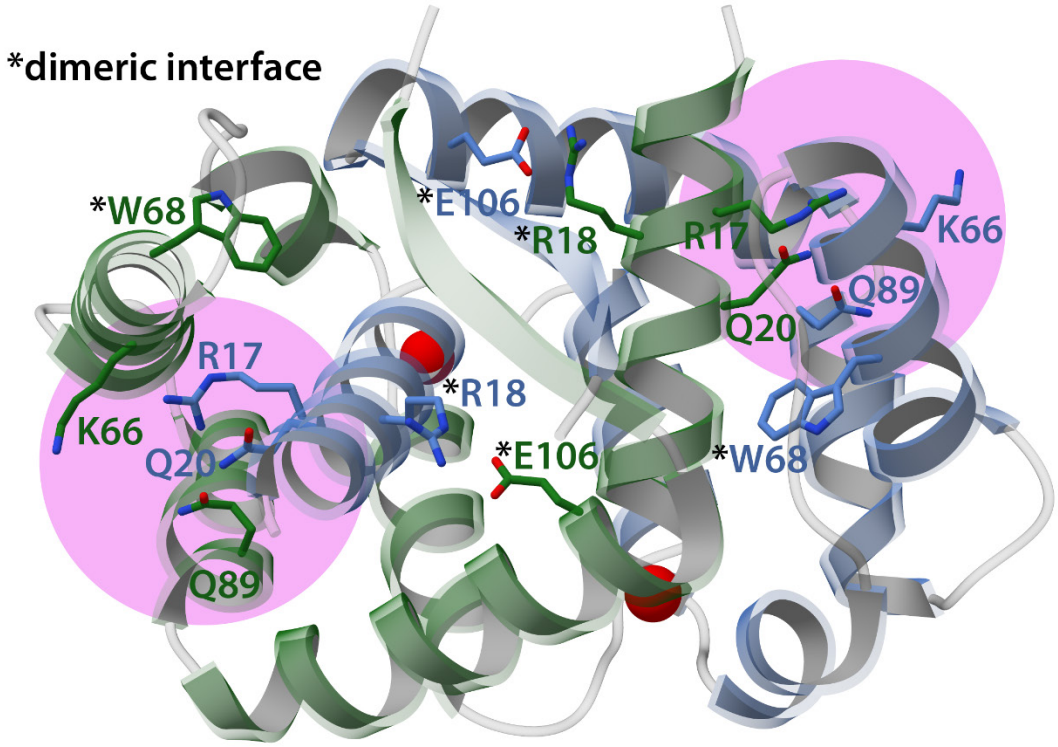

Supplementary Figure 8 | DurN residues selected for site-directed mutagenesis. DurN activity is abolished upon mutating the selected residues (drawn as sticks) to Ala (i.e. R17A, R18A, Q20A, K66A, W68A, Q89A, and E106A). Loss in activity is attributed either to compromising substrate recognition or disruption of the homodimer interface. Residues involved in intermonomer contacts at the dimer interface are highlighted with an asterisk. A magenta circle is drawn to encapsulate residues important for substrate recognition. Potassium ions are represented as red spheres.

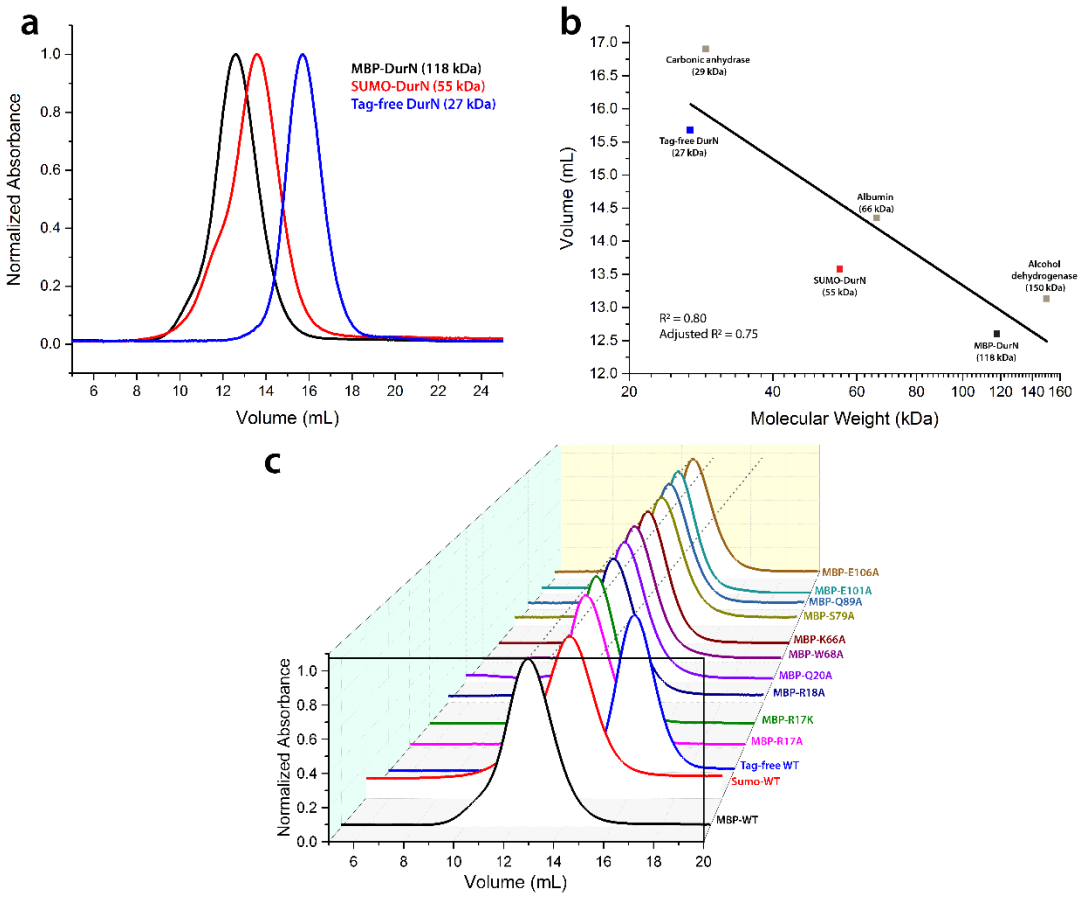

Supplementary Figure 9 | Analytical gel-filtration analysis of DurN and its variants. a, Overlaid chromatograms of MBP-DurN, Sumo-DurN, and tag-free wild-type DurN analyzed by size-exclusion chromatography. **b,** Wild-type DurN fusions and tag-free protein plotted on a standard curve generated using protein standards suggests that DurN forms a dimer in solution both as stand-alone protein or with N-terminal MBP and Sumo tags. Single replicate measurements ($n = 1$) are plotted and the R-squared and adjusted R-squared values are reported for the linear best fit. **c**, Overlaid chromatograms of all DurN variants in this study. Co-elution of similarly tagged variants suggests the single amino acid substitutions do not abrogate dimerization, in accord with the high degree of intermolecular contacts resulting in a large surface area at the interface of the homodimer observed in all DurN crystal structures. All experiments were performed once on the same day. The mutants elute as expected and clearly behave the same as the wild type and hence dimerization does not seem to be affected by these mutations.

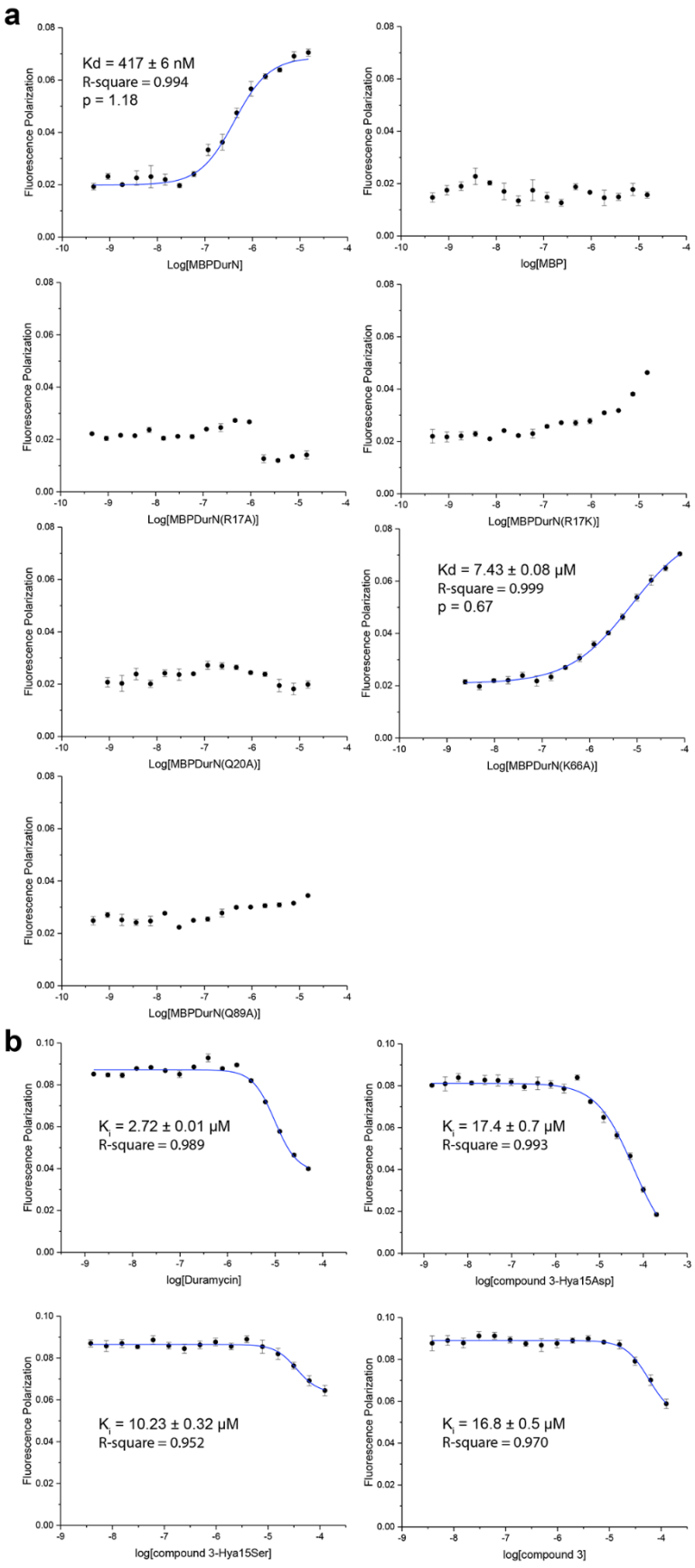
a
Kd = 417 ± 6 nM
R-square = 0.994
p = 1.18
Log[MBPDurN]
log[MBP]
Log[MBPDurN(R17A)]
Log[MBPDurN(R17K)]
Kd = 7.43 ± 0.08 μM
R-square = 0.999
p = 0.67
Log[MBPDurN(Q20A)]
Log[MBPDurN(K66A)]
Log[MBPDurN(Q89A)]
Fluorescence Polarization
b
K$_i$ = 2.72 ± 0.01 μM
R-square = 0.989
log[Duramycin]
K$_i$ = 17.4 ± 0.7 μM
R-square = 0.993
log[compound 3-Hya15Asp]
K$_i$ = 10.23 ± 0.32 μM
R-square = 0.952
log[compound 3-Hya15Ser]
K$_i$ = 16.8 ± 0.5 μM
R-square = 0.970
log[compound 3]

Supplementary Figure 10 (previous page) | Fluorescence polarization (FP) and competition FP binding studies. a, FP analysis of **Dur-FL** binding to MBP-DurN, MBP, and MBP-DurN variants. **b,** Competition FP analysis of the **Dur-FL** and MBP-DurN complex competed with duramycin, **3**-Hya15Asp, **3**-Hya15Ser, and **3**. Data shown are the means from two or three independent experiments where error bars represent the standard errors of mean. Dur-FL binding to MBP-DurN(R17K), MBP-DurN(Q29A), MBP-DurN(K66A), MBP-DurN(Q89A), were performed in two independent experiments (n = 2). All other binding or inhibition analysis were performed in three independent experiments (n = 3). R-squared values are reported for a dose-response curve fit (see Methods for the equation).

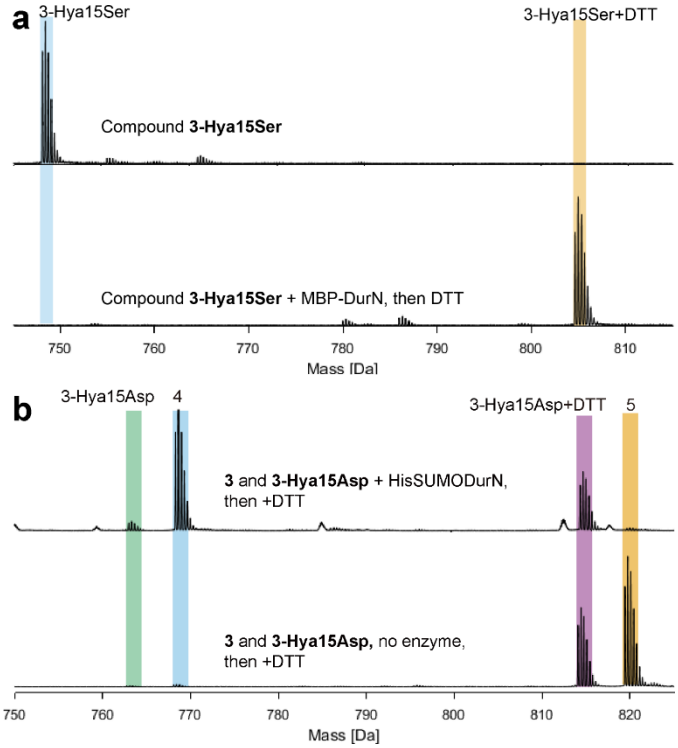

Supplementary Figure 11 | *In vitro* activity assays with DurN and substrate analogs. a, Electrospray ionization mass spectrometry (ESI-MS) of **3**-Hya15Ser (top) incubated with MBP-DurN, then treated with DTT (bottom). **b,** Compound **3** and **3**-Hya15Asp incubated with Sumo-DurN (top) or no enzyme (bottom), then treated with DTT to stop the reactions. Unreacted compound **3**-Hya15Asp is colored in green, product **4** formed from **3** is colored in blue, DTT added to **3**-Hya15Asp is colored in purple, and to **3** (compound **5**) is colored in orange. The competition assay shows that **3** is a much better substrate for DurN than **3**-Hya15Asp. All experiments were performed three independent times with similar results.

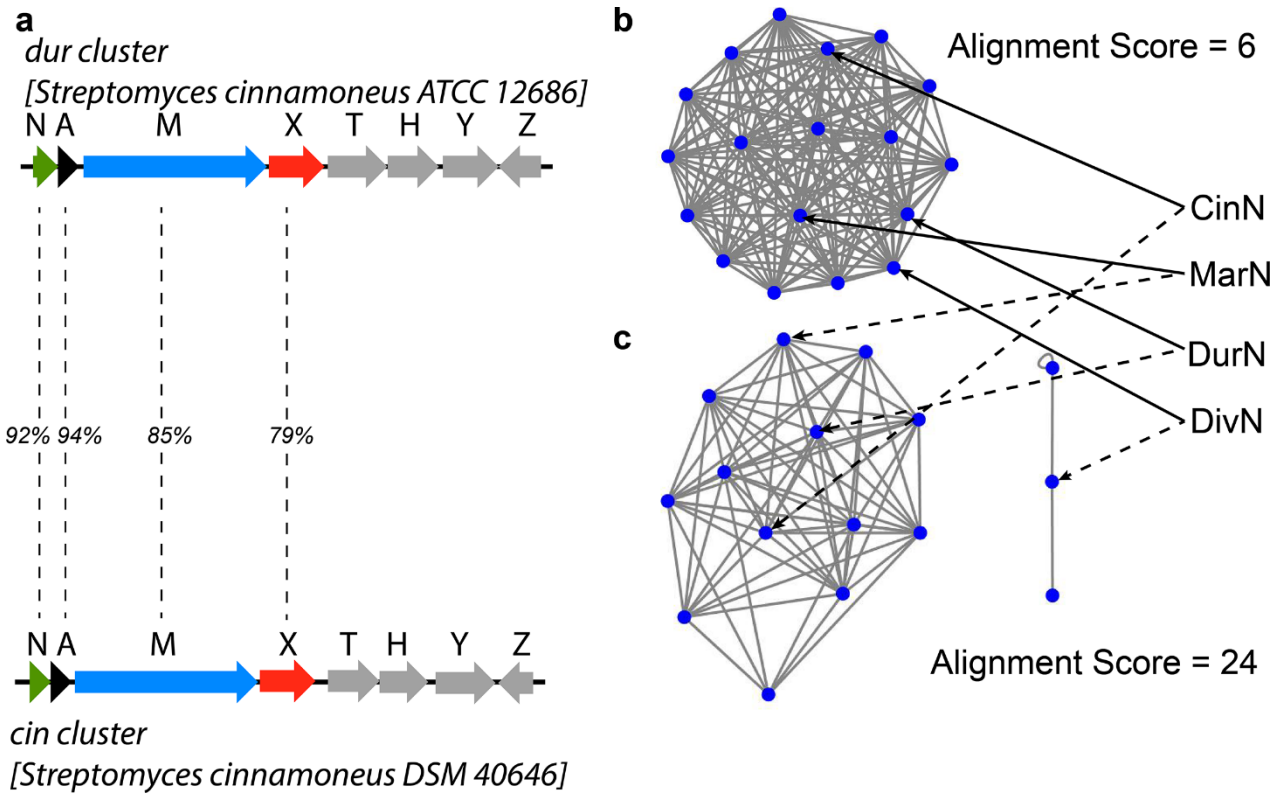

Supplementary Figure 12 | Comparison of DurN and its homologs identified by a BLAST search. a, Comparison of duramycin and cinnamycin biosynthesis clusters, the identities between proteins from the minimum biosynthesis cassette are marked in the middle. **b,** sequence similarity network (SSN) of DurN. Enzymes that are involved in the biosynthesis of characterized natural products are labeled. Family members were identified by BLAST with DurN as query and an E-value of 10^{-5} as cut-off. Sequence identity and coverage is > 38% and 86%, respectively. The networks were generated with alignment scores of 6 and 24. Only at high alignment scores do members of the family separate.